TRANSPORTATION POOLED FUND PROGRAM
QUARTERLY PROGRESS REPORT

Lead Agency (FHWA or State DOT): ____Kansas DOT_____

INSTRUCTIONS:

Project Managers and/or research project investigators should complete a quarterly progress report for each calendar quarter during which the projects are active. Please provide a project schedule status of the research activities tied to each task that is defined in the proposal; a percentage completion of each task; a concise discussion (2 or 3 sentences) of the current status, including accomplishments and problems encountered, if any. List all tasks, even if no work was done during this period.

Transportation Pooled Fund Program Project # **TPF-5(328)**	**Transportation Pooled Fund Program - Report Period:** ☐Quarter 1 (January 1 – March 31) ☐Quarter 2 (April 1 – June 30) ☒Quarter 3 (July 1 – September 30) ☐Quarter 4 (October 1 – December 31)
Project Title: Strain-based Fatigue Crack Monitoring of Steel Bridges using Wireless Elastomeric Skin Sensors	
Project Manager: David Behzadpour Phone: (785) 291-3847 E-mail: David.Behzadpour@ks.gov	
Project Investigator: Li Jian Phone: 785-864-6850 E-mail: jianli@ku.edu	

Lead Agency Project ID: **RE-0699-01**	**Other Project ID (i.e., contract #):**	**Project Start Date:** **9/2015**
Original Project End Date: **Multi-year project**	**Current Project End Date:** **8/31/2018**	**Number of Extensions:** **N.A.**

Project schedule status:

☒ On schedule ☐ On revised schedule ☐ Ahead of schedule ☐ Behind schedule

Overall Project Statistics:

Total Project Budget	Total Cost to Date for Project	Total Percentage of Work Completed
$405,000	**$ 405,000**	**100%**

Quarterly Project Statistics:

Total Project Expenses This Quarter	Total Amount of Funds Expended This Quarter	Percentage of Work Completed This Quarter
$ 46,733	**$ 46,733**	**9%**

Project Description:
The main objective of this proposed research is to *provide state DOTs a practical and cost-effective long-term fatigue crack monitoring methodology using* ***a wireless elastomeric skin sensor network****.* This research is intended to demonstrate the value-added of fatigue crack monitoring of steel bridges using wireless skin sensors over the traditional bridge inspection.

Progress this Quarter (includes meetings, work plan status, contract status, significant progress, etc.):

In order to validate the integrated wireless fatigue crack monitoring system, in this quarter, a field deployment is conducted for the I-70 steel highway bridge which is subject to fatigue damage. Several wireless elastomeric skin sensors were deployed over fatigue-susceptible regions at the midspan in a steel girder. Particularly, two sizes of SECs including large SEC with 3 in. by 3 in. (76.2 mm by 76.2 mm) and small SEC with 1.5 in. by 1.5 in. (38.1 mm by 38.1 mm) were selected for installation. The newly-developed wireless capacitive sensing boards were also deployed for measuring the capacitances of the SECs under traffic loads. The system ran autonomously and collected a large number of data sets triggered by the passing vehicles. Data collected in this field deployment indicates the SEC's measurement can be collected under passing vehicles, hence form the basis for long-term monitoring of fatigue critical steel bridges.

Anticipated work next quarter:

The final report has been completed and is currently being internally reviewed. After the internal review, it will be submitted to KDOT for approval.

Significant Results:

1. Descriptions of the field deployment

1.1. The Test bridge

The test steel bridge was a part of the I-70 highway near Kansas City, Kansas, at the intersection of the N. 57th Street, as illustrated in Fig. 1a. According to the inspection reports provided by the Kansas Department of Transportation (KDOT), the bridge was named 70-105-41731-127 (westbound) and 70-105-41732-128 (eastbound) and was originally designed in 1984 with some repairs in 2004. The bridge has 8 spans with an overall length of 680 ft. Based on the recent two inspections performed in 2013 and 2017, respectively, multiple locations on the bridge was subject to fatigue damage, typically at web-gap regions in the cross-frame-to-girder connections, as shown in Figure b.

Fig. 1 shows a typical web-gap region with existing fatigue cracks. Driven by the out-of-plane movement of the cross frame, a fatigue crack initiated at the top end of the weld between the connection plate and girder web. Depending on the structural layout, the fatigue crack could either grow along the weld toe or propagate into the girder web.

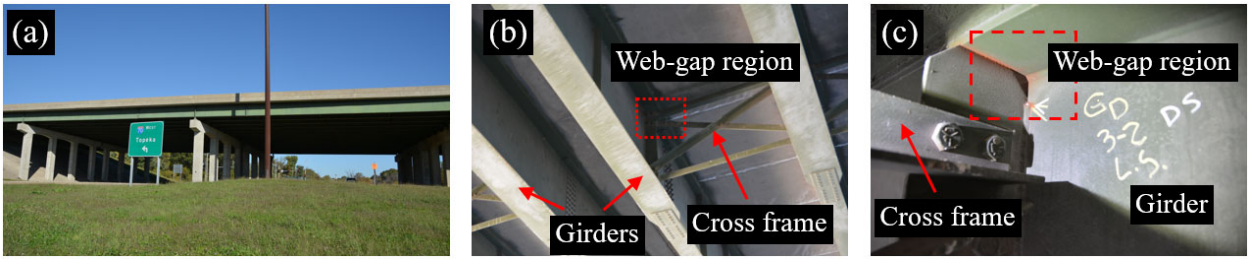

Figure 1. (a) The test bed bridge in the field; (b) Typical cross frame and longitudinal girders; and (c) Web-gap region between the cross frame and the girder.

To facilitate the field deployment, a man-lift truck was adopted. The man-lift platform can easily access the fatigue-susceptible regions in the steel girders. A power generator was also used for offering electric power during the deployment. Fig. 2 shows some photos taken during the field visits.

Figure 2. Field deployment of the monitoring system on a steel bridge.

6.4.2 SEC arrangement

An exterior girder was selected for the SEC installation, as shown in Figure 3a. Two fatigue-susceptible regions were selected for the SECs. The first region is on the web gap region on the exterior side of the girder (Fig. 3b). This region was inspected in both 2013 and 2017. Based on the inspection reports and the marks on the structural surface, two fatigue cracks can be found in this region including: 1) a horizontal crack initiated between the flange and the web (Crack 1); and 2) a horizontal crack in the web (Crack 2). As can be seen in Fig. 3**Figure** c, both cracks propagated during the period between the past two inspections.

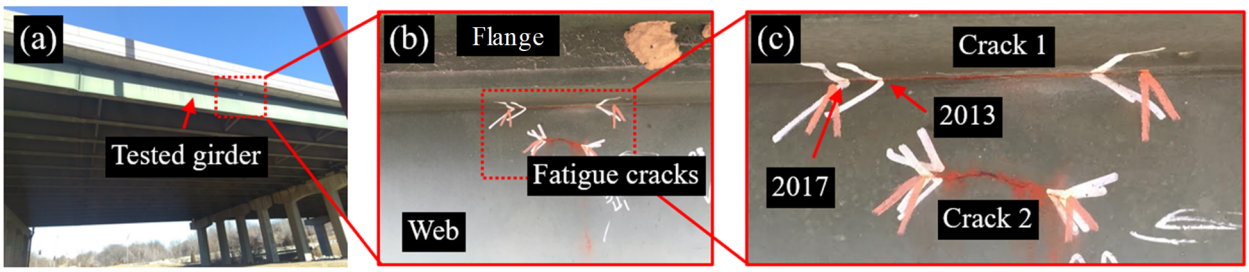

Figure 3. Detail views about the exterior side of the girder prior to the sensor installation. (a) the steel girder for sensor deployment; (b) two fatigue cracks at the exterior side of the girder; and (c) different arrows indicate crack growths at different inspection periods.

Fig. 4 demonstrates the arrangement of the SECs where 5 small SECs with a size of 1.5 in. by 1.5 in. (38.1 mm by 38.1 mm) were deployed in this region. In particular, two SECs (a1 and a5) were installed to cover Crack 1 and three SECs (a2, a7, and a4) were attached to Crack 2. Additional short cables were attached to the SECs in order to connect them to the wireless capacitive board for data collection, as shown in Fig. 4b.

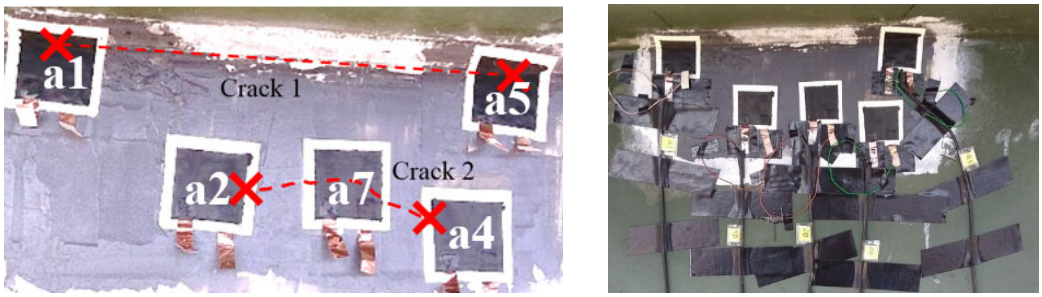

(a) **(b)**

Figure 4. (a) Arrangement of the SEC arrays; and (b) the SEC arrays after soldering the cables.

Fig. 5a illustrates the SEC installation on same web-gap region in the interior side of the girder. A fatigue crack (Crack 3) was observed between the connection plate between the cross frame and the girder web. One large SEC was installed in this region, denoted as SEC b1 as shown in Fig. 5b.

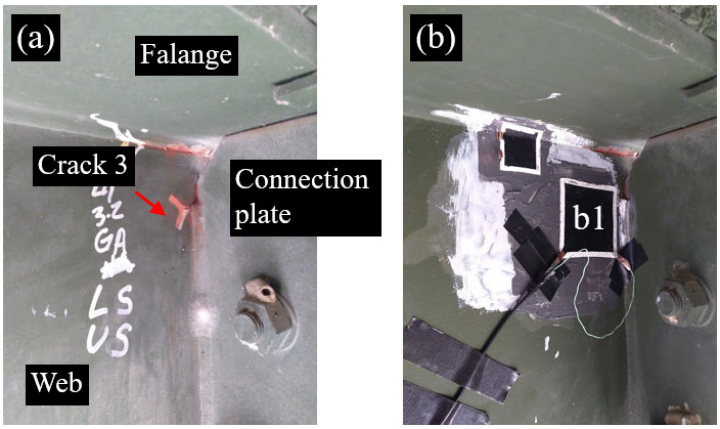

Figure 5. SEC installation on the interior side of the girder. (a) The chosen fatigue-susceptible region prior to the installation; and (b) SEC installation.

6.4.3 Strain gauge installation

To normalize the capacitance measurement of the SEC, the loading information due to the passing vehicles are needed. In this field deployment, we adopted strain measurements from the cross frame to indirectly infer the traffic load. Fig. 6 shows the strain gauge installation for which the cross frame near the web-gap region was selected for the strain gauge deployment. The strain gauge was installed at the bottom chord of the cross frame, as shown in Fig. 6b.

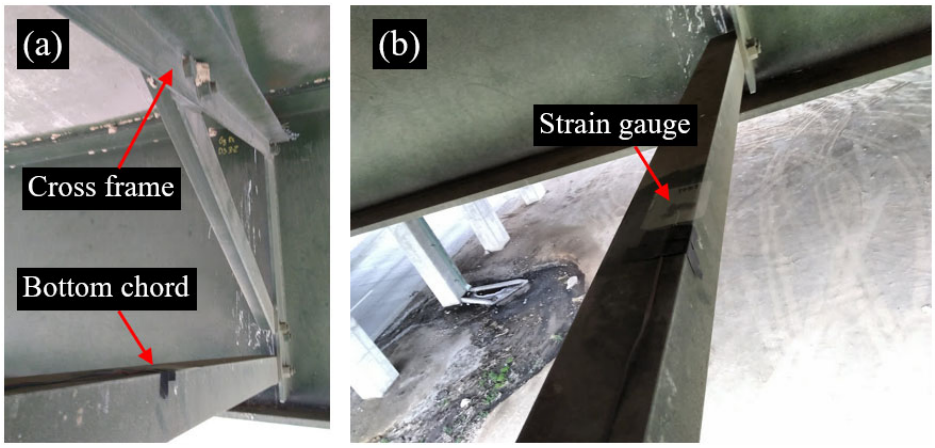

Figure 6. SEC installation on the interior side of the girder. (a) fatigue-susceptible region prior to the installation; and (b) SEC installation.

2. Deployment of wireless capacitive sensing boards

The manufactured sensor boards were shipped from Arizona team to KU. The sensor boards were all tested for quality assurance at KU as well. During a field visit, we measured the nominal capacitances of all SECs installed on the bridge mid-span. We used the measured nominal capacitances to pre-balance all the sensor boards and calculate their Shunt calibration coefficients. Thus, in our final deployment, we would just need to connect the SECs to the sensor boards. Fig. 7 presents the schematic of sensor deployment on the bridge for the exterior and interior sides of the girder together with their nominal capacitances. Table 1 shows the assigned pre-balanced sensor board to each SEC sensor and their corresponding Shunt calibration coefficients calculated in the lab.

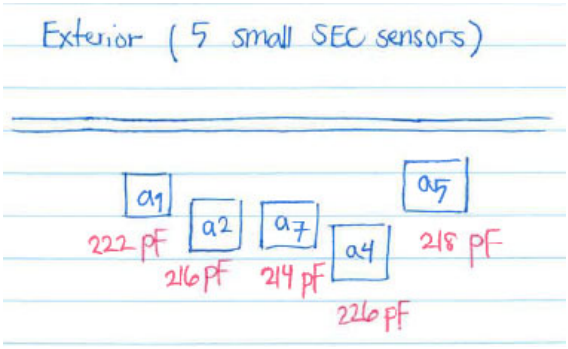

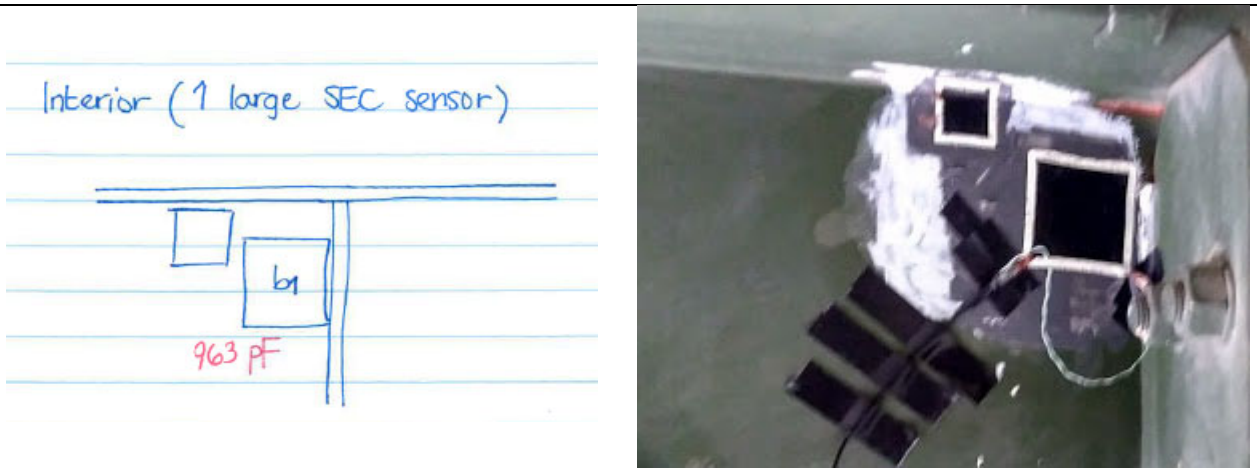

Figure 7. Schematic of sensor layout on the bridge

Table 1. Connection details for the final deployment on the test bridge

Girder face	SEC Sensor		Sensor board	Shunt calibration coefficient (V/pF)	Breakout box	Breakout box calibration	Xnode	Channel number
Exterior	Small SEC	a1	S4	0.005109	No. 2	7.6613	Node 5	4
		a2	S8	0.008775				5
		a5	S3	0.031253				8
		a7	S10	0.043672				6
	Strain	-	-	-				7
Interior	Large SEC	b1	L2	0.001211	No. 1	7.6725	Node 1	8
	Strain	-	-	-				7

The final task for field deployment was to incorporate the breakout box which is an interface to connect the Xnode's sensing channels to the sensor boards for wireless data collection. Fig. 8 shows the interface board inside the breakout box. This board works as an interface between Xnode and sensor boards to allow integration of the sensor boards to the external channels of Xnode. The breakout box itself has a calibration coefficient for voltage measurements. To calculate the coefficient, we first took measurements from one SEC sensor using the Xnode through the breakout box and the NI-DAQ, respectively. We then matched these two measurements to compute the coefficient. An example of measurements from both Xnode and NIDAQ are shown in Fig. 9 before and after applying the calibration coefficient. For this particular breakout box, the coefficient is equal to 7.66. It can be seen that after applying the coefficient, the measured signal from Xnode and the breakout box matches pretty well with the measurement from NIDAQ. Note that the plotted signal after the calibration coefficient is a zoom-in version of the original signal.

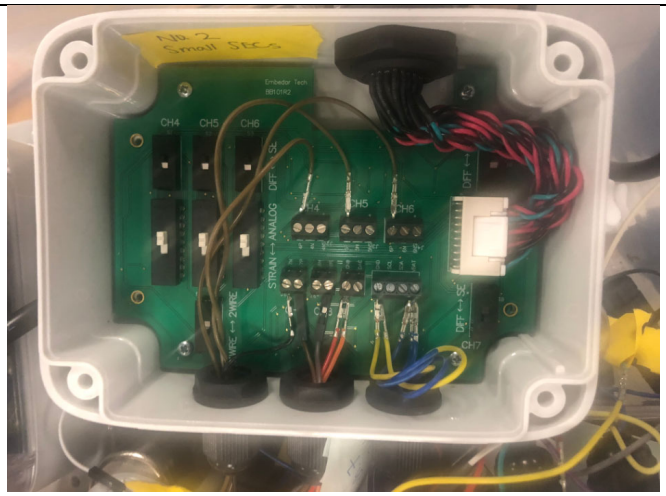

Figure 8. The breakout box

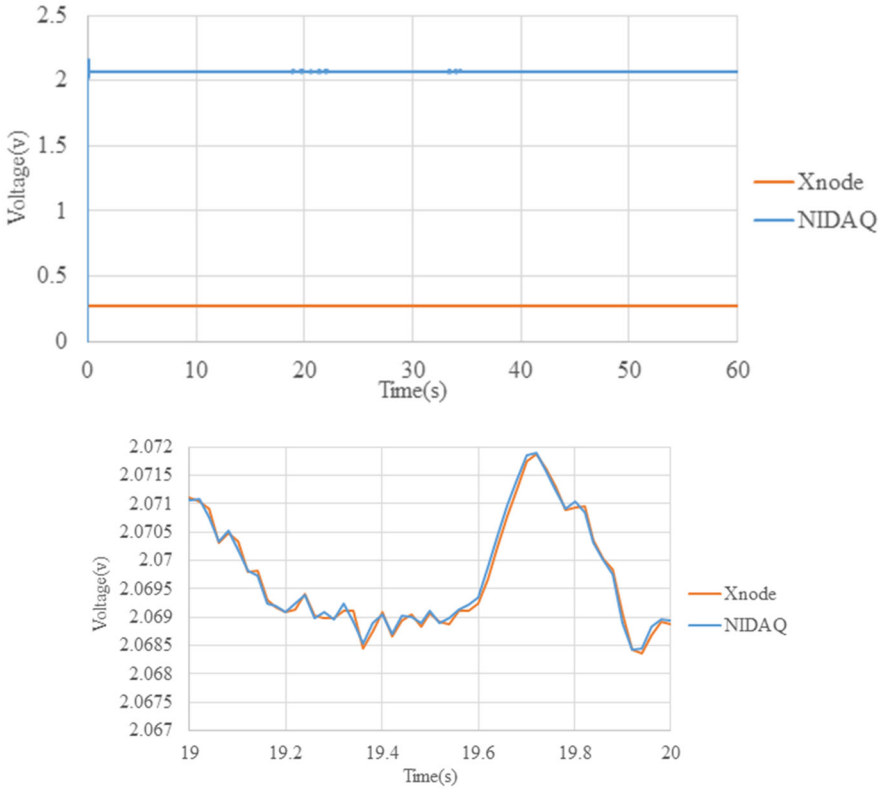

Figure 9. An example of calculation of the breakout box calibration coefficient

Fig. 10 shows how we used the breakout box to make all the connections required between the Xnode and the sensor boards. The breakout box is connected to the Xnode through a cable, and the sensor boards are connected to the breakout box through a series of jumper wires. In the field, we would just need to connect the SEC sensors to the sensor boards. The details of the connections between the sensor boards, breakout boxes, and Xnode channels for the final deployment are described in Table 1.

Figure 10. Connection of sensor boards to Xnode through the breakout box

Fig. 11 shows a picture of the final sensor deployment on the bridge. For this deployment, on the facial side of the girder, measurements are taken from 4 small SEC sensors and one strain gauge. On the interior side, one large SEC sensor is connected to an Xnode for measurements.

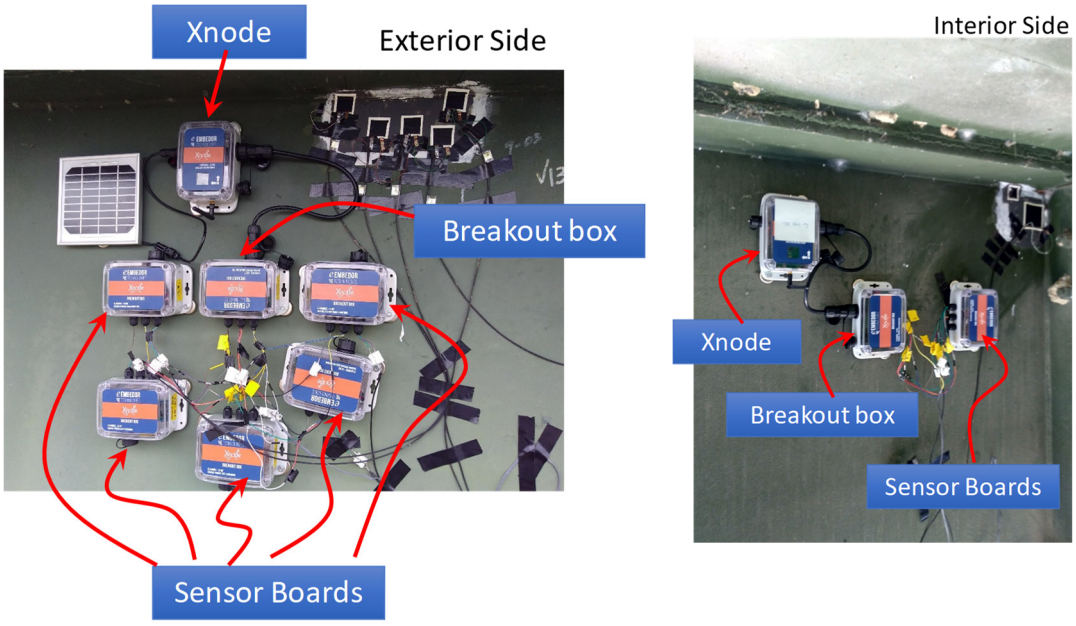

Figure 11. Sensor layout of the field deployment on 07/16/2018

3. Analysis of data collected from the field deployment

3.1 Results from the exterior side of the girder

Once the monitoring system was deployed in the steel bridge, measurements were autonomously collected from the Xnode under the traffic loads between July 16th and 17th, 2018. The datasets collected in the exterior side of the girder include: 1) measurements from the strain gauge on the cross frame; 2) measurements of SEC a1, a2, a3, and a5 on the fatigue-susceptible region; and 3) the acceleration responses of the girder. All measurement are synchronized with a duration of 1 min.

Fig. 12 shows a typical dataset from the exterior side of the girder where more measurements can be found in Appendix D.1. The acceleration measurement is demonstrated in Fig. 12a, where several peaks can be found within the one minute measurement. Similarly, the strain measurement also shows peaks at approximately the same locations. These

results indicate that both the accelerometer and strain gauge can identify the responses caused by the passing vehicles. Notice that strain measurement has low resolution compared with acceleration measurement. This is probably due to quantization error in the strain sensing board.

Fig. 12b to Fig. 12f show the capacitance measurements of the SECs. As can be seen in the figures, SEC a5 produces a very small response compared with other three SECs. On the other hand, SEC a1, a2, and a3 have larger responses but the signals contain two major components including; 1) high-frequency components at the approximate locations when acceleration and strain measurements have large responses due to the traffic loads; 2) low-frequency components throughout the time-series. The first component could be provoked by the traffic load; while the second component is probably caused by the magnetic interference in the field which is not relevant to the traffic loading.

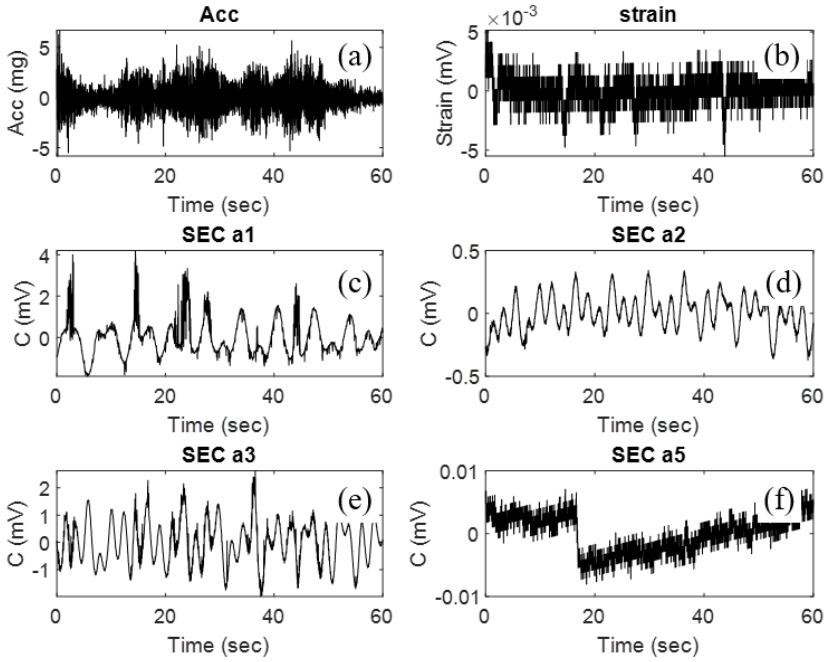

Figure 12. Typical measurements from the exterior side of the girder. (a) acceleration; (b) strain; (c) SEC a1; (d) SEC a2; (e) SEC a3; and (f) SEC a5.

To further remove the low-frequency content while keeping the high frequency responses, a curve fitting technique is applied to fit the low-frequency component. The fitted curve is shown as a red line and the original data of SEC a1 is illustrated as blue dots in Fig. 13a. Next, by subtracting the original data with the fitted curve, the high frequency signal of SEC a1 can be extracted, as shown in Fig. 13b.

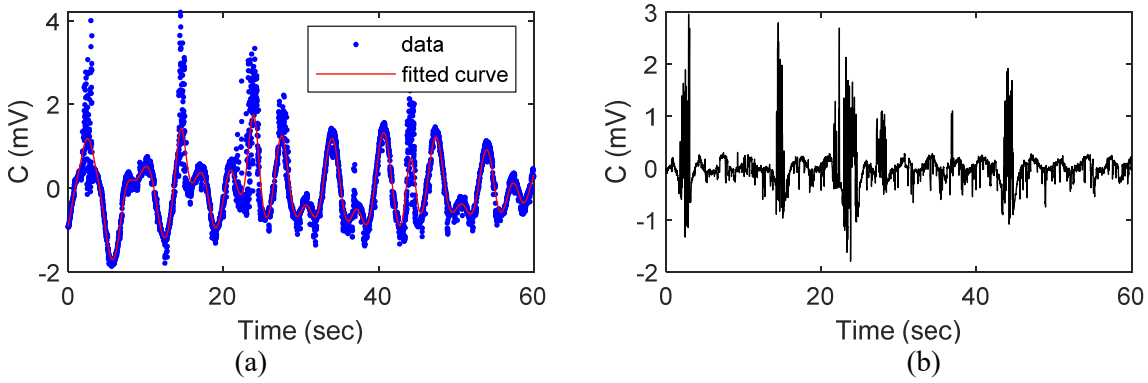

Figure 13. (a) curve fitting of SEC a1; and (b) SEC a1's response after removing the low-frequency content

Using this strategy, the capacitance measurement of SEC a2 can be processed and the result can be found in Fig. 14. Fig. 15 shows the results of SEC a3. The high frequency peaks can be reserved after removing the low-frequency content, as shown in Fig. 15b.

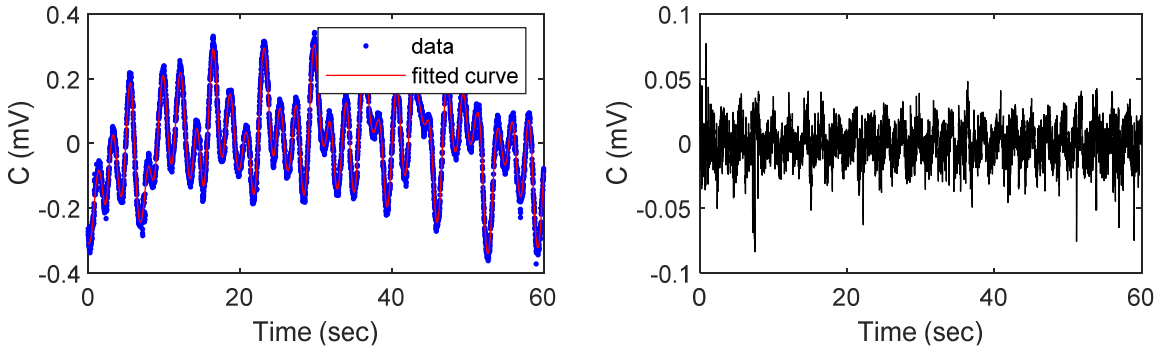

Figure 14. (a) curve fitting of SEC a2; and (b) SEC a2's response after removing the low-frequency content

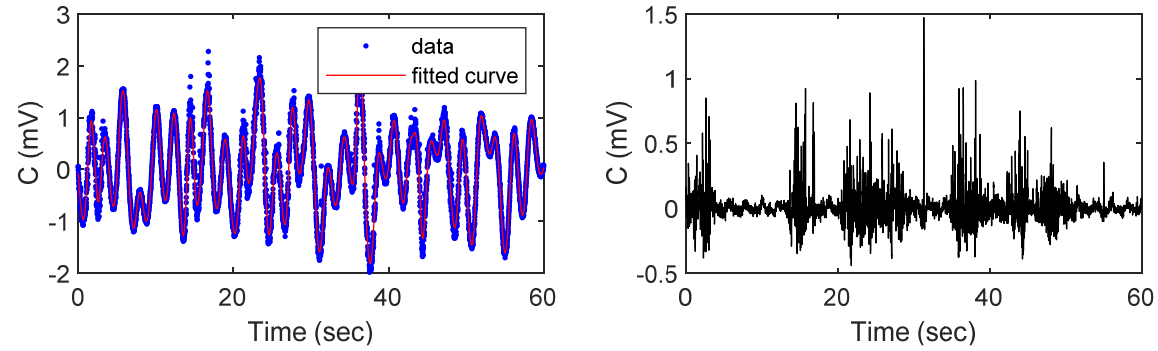

Figure 15. (a) curve fitting of SEC a3; and (b) SEC a3's response after removing the low-frequency content

3.2 Results from the interior side of the girder

The datasets collected in the interior side of the girder include: 1) measurements of the strain gauge on the cross frame; 2) measurements of a large SEC on the fatigue-susceptible region; and 3) accelerations of the girder. All measurement are synchronized with a duration of 1 min.

Fig. 16 shows the typical measurements of interior side of the girder. Several regions of high responses can be found in the acceleration measurement, as shown in Fig. 16a. Strain and SEC signals also demonstrate responses with relatively higher amplitudes. Low frequency drifts can be found in the SEC and strain measurements.

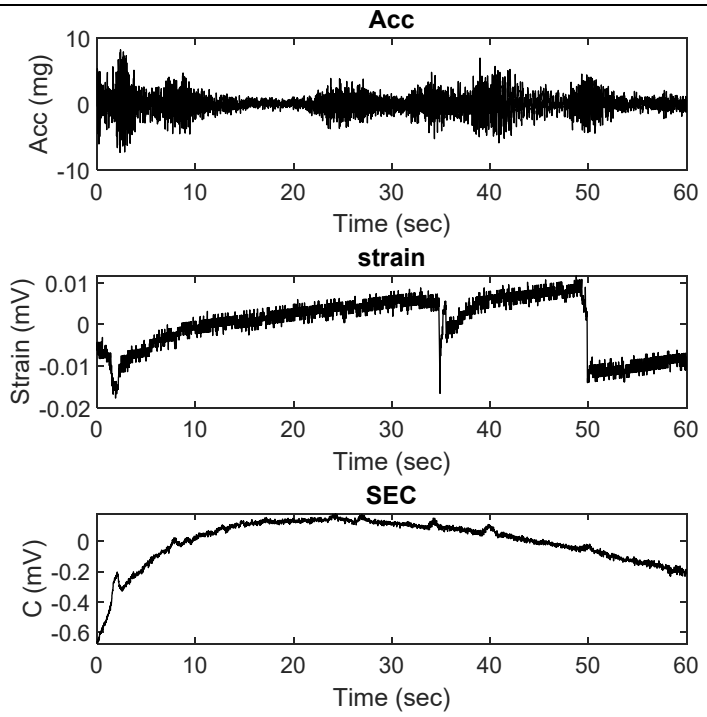

Figure 16. Typical measurements from the interior side of the girder. Top: acceleration; middle: strain; and bottom: SEC.

3.3 Crack growth index

Using the previously developed algorithm, Crack growth indices (CGI) can extracted from the field measurements of SECs. For the SEC measurements in the exterior side of the girder, low-frequency components exist in the measurements caused by noise. Extracting CGIs would be difficult as the SEC responses provoked by the traffic loads share the similar frequency content as the noise. Hence, in this subsection, only CGIs from the large SEC at the interior side of the girder are extracted.

To compute the CGI, the power spectral densities (PSDs) of acceleration, strain, and SEC measurements are extracted first. As can be found in Fig. 17, a peak is located in the higher frequency range of the acceleration PSD curve, while peaks in the strain and SEC's PSDs are at low frequency ranges. Notice that these lower PSD peaks in strain and SEC are caused by the passing traffic loads and drifts in the time series signals.

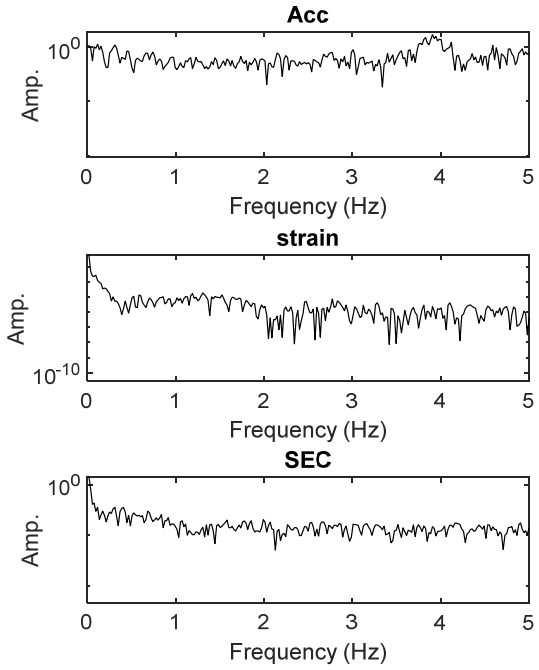

Figure 17. Power spectral densities (PSDs) of acceleration, strain, and SEC measurements.

To remove the effect of drifts, a cut-off window is applied to the PSD results of the strain and SEC measurements, respectively. The range of the cut-off window is from 0.2 Hz to 0.8 Hz. These values would keep the meaningful results in the PSDs caused by traffic loads. Meanwhile, the extremely low-frequency content can be removed by selecting 0.2 Hz as the lower bound of the window. The PSD of strain measurement after the cut-off can be found in Fig. 18a. With a similar cut-off window, the PSD of SEC measurement after cut-off can be found in Fig. 19a.

Next, a moving-average low-pass filter is applied to the PSD results. This filter would smooth the PSD curves so that the magnitude of PSD can be more reliably estimated. Results after applying the moving average filter can be seen in Fig. 18b and Fig. 19b.

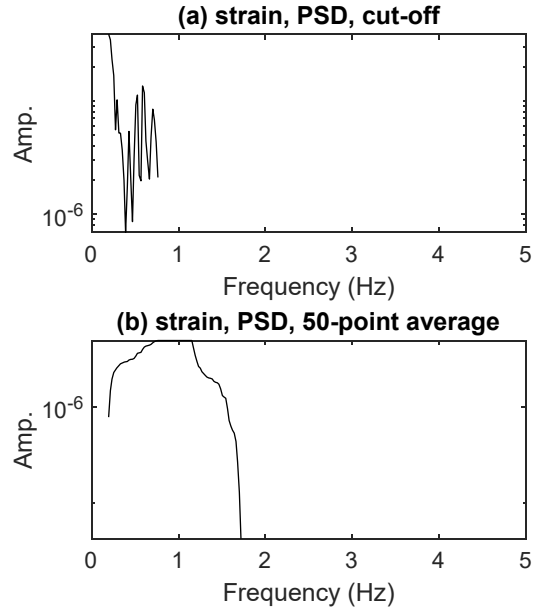

Figure 18. (a) PSD result of the strain measurement after cut-off; and (b) result after applying a low pass filter.

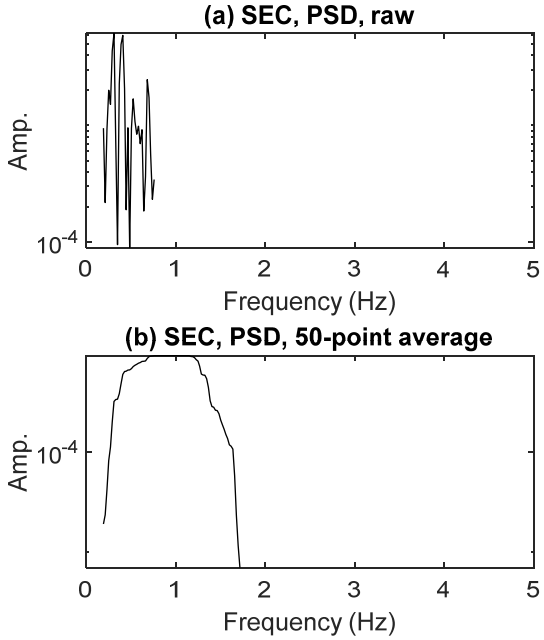

Figure 19. (a) PSD result of the SEC measurement after cut-off; and (b) result after applying a low pass filter.

Once the filtered PSD curves of strain and SEC measurements are obtained, the CGI can be calculated. Fig. 20 shows the final CGI result of the large SEC. Notice that only the flat platform around 1 Hz is of interest, as this frequency range is caused by the passing traffic loads. In this regard, the CGI of the large SEC is about 14.

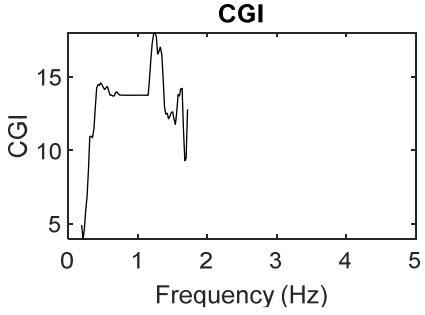

Figure 20. CGI of the large SEC.

3.4 Statistical analysis of Crack growth index

During the field visits on July 16th and 17th, 817 datasets of the large SEC on the interior side of the girder were autonomously collected by the wireless monitoring system. Utilizing the similar approach shown above, 817 datasets are processed such that CGIs of all datasets can be obtained. Fig. 21 shows the CGI results where most CGIs have the magnitudes around 20, while a few datasets produce smaller or larger CGI values. This variation could be attributed to the noise content and low frequency drifts in the strain and SEC measurements.

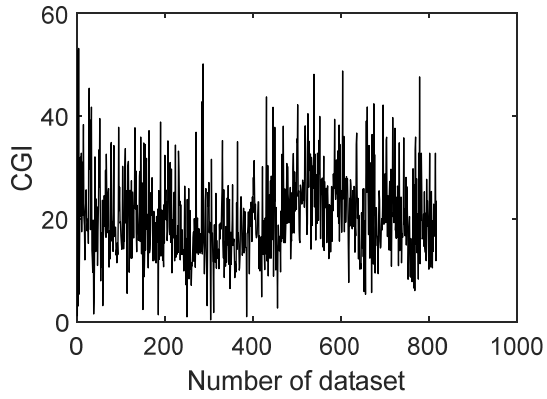

Figure 21. CGIs of 817 datasets of the large SEC.

Fig. 22 shows the histogram of the CGIs shown in Fig. 21. As can be seen in the figure, the majority of CGIs are within 10 to 30. This indicates that the proposed CGI approach is able to extract meaningful features from the field measurements. By continuing to collect the data in the field over long-term, it would be feasible to establish multiple histogram of CGIs at different data collection periods. The fatigue crack growth would be monitored through the histogram of CGIs.

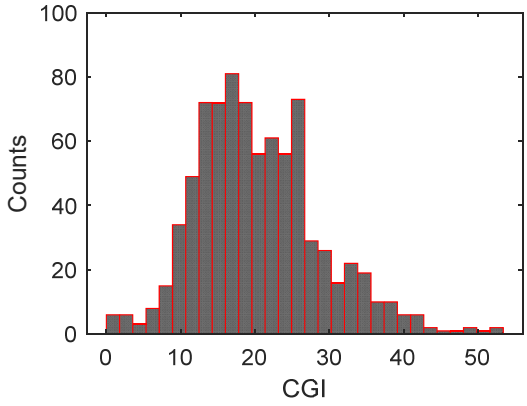

Figure 22. Histogram of CGI results in Figure 21.

Circumstance affecting project or budget. (Please describe any challenges encountered or anticipated that might af the completion of the project within the time, scope and fiscal constraints set forth in the agreement, along with recommended solutions to those problems).

None.